Revisiting Emission-line Measurement Methods for Narrow-line Active Galactic Nuclei

Viraja C. Khatu[1] , Sarah C. Gallagher[1] , Keith Horne[2] , Edward M. Cackett[3] , Chen Hu[4], Pu Du[4] , Jian-Min Wang[4] , Wei-Hao Bian[5] , Jin-Ming Bai[6], Yong-Jie Chen[4], Patrick Hall[7], Bo-Wei Jiang[4], Sha-Sha Li[6] , Yan-Rong Li[4] , Sofia Pasquini[8] , Yu-Yang Songsheng[4], Chan Wang[5], Ming Xiao[4], and Zhe Yu[4]

[1] Department of Physics and Astronomy & Institute of Earth and Space Exploration, The University of Western Ontario, 1151 Richmond Street, London, ON N6A 3K7, Canada; vkhatu@uwo.ca
[2] School of Physics and Astronomy, University of St Andrews, North Haugh, St Andrews, KY16 9SS, UK
[3] Department of Physics & Astronomy, Wayne State University, 666 West Hancock Street, Detroit, MI 48201, USA
[4] Key Laboratory for Particle Astrophysics, Institute of High Energy Physics, Chinese Academy of Sciences, 19B Yuquan Road, Beijing 100049, People's Republic of China
[5] Physics Department, Nanjing Normal University, Nanjing 210097, People's Republic of China
[6] Yunnan Observatories, The Chinese Academy of Sciences, Kunming 650011, People's Republic of China
[7] Department of Physics and Astronomy, York University, 4700 Keele Street, Toronto, ON M3J 1P3, Canada
[8] Department of Physics and Astronomy, The University of Western Ontario, 1151 Richmond Street, London, ON N6A 3K7, Canada
Received 2022 December 31; accepted 2023 March 31; published 2023 May 2

Abstract

Measuring broad emission-line widths in active galactic nuclei (AGN) is not straightforward owing to the complex nature of flux variability in these systems. Line width measurements become especially challenging when the signal-to-noise ratio is low, profiles are narrower, or spectral resolution is low. We conducted an extensive correlation analysis between emission-line measurements from the optical spectra of Markarian 142 (Mrk 142; a narrow-line Seyfert galaxy) taken with the Gemini North Telescope (Gemini) at a spectral resolution of $185.6 \pm 10.2 \, \mathrm{km \, s^{-1}}$ and the Lijiang Telescope (LJT) at $695.2 \pm 3.9 \, \mathrm{km \, s^{-1}}$ to investigate the disparities in the measured broad-line widths from both telescopes' data. Due to its narrow broad-line profiles, which were severely affected by instrumental broadening in the lower-resolution LJT spectra, Mrk 142 posed a challenge. We discovered that allowing the narrow-line flux of permitted lines having broad and narrow components to vary during spectral fitting caused a leak in the narrow-line flux to the broad component, resulting in broader broad-line widths in the LJT spectra. Fixing the narrow-line flux ratios constrained the flux leak and yielded the Hβ broad-line widths from LJT spectra ∼54% closer to the Gemini Hβ widths than with flexible narrow-line ratios. The availability of spectra at different resolutions presented this unique opportunity to inspect how spectral resolution affected emission-line profiles in our data and adopt a unique method to accurately measure broad-line widths. Reconsidering line measurement methods while studying diverse AGN populations is critical for the success of future reverberation-mapping studies. Based on the technique used in this work, we offer recommendations for measuring line widths in narrow-line AGN.

Unified Astronomy Thesaurus concepts: Active galactic nuclei (16); Spectroscopy (1558)

Online material: color figures

1. Introduction

Observing gaps in multi-epoch astronomical data are commonplace. Sparsely sampled ground-based observations are mainly a result of weather conditions and pressure from other programs (for queue observatories). Data gaps can impact the programs requiring frequent visits to the sky, e.g., time-series observations. One way to work around data gaps is by performing simultaneous observations with different telescopes. However, using data from various observatories together in a meaningful way can be challenging because of the need for sufficient cross-calibration.

Combining spectroscopic observations from different facilities requires careful consideration of various factors (e.g., exposure time, seeing, spectral resolution, etc.) affecting the data. When employing multiple telescopes to observe the same spectral region for a given data set, the instrument specifications used with different facilities may not be identical. As an example, if the data from two telescopes were taken with different slit widths, their spectral resolutions may not match.

The wider the slit, the lower the spectral resolution (depending on the grating used). Instrumental broadening in lower-resolution spectra causes line features to appear broader than the true value or sometimes blended with neighboring lines. This broadening effect can result in inaccurate measurements of the physical parameters, e.g., the FWHM and flux of an emission line. However, the severity of the effect may be different for different studies. For objects showing broad-line profiles considerably narrower than the typical active galactic nucleus (AGN) population, e.g., narrow-line Seyfert 1 galaxies (NLS1s) accreting at super-Eddington rates, accounting for instrumental broadening effects while performing line measurements becomes more critical.

Historically, reverberation-mapping (RM; Blandford & McKee 1982; Peterson 1993) studies have focused mainly on low-redshift AGN ($z < 0.3$) that typically follow sub-Eddington accretion (e.g., Stirpe et al. 1994; Santos-Lleó et al. 1997; Collier et al. 1998; Dietrich et al. 1998; Kaspi et al. 2000; Bentz et al. 2006) instead of the more atypical super-Eddington objects (accreting well above the Eddington limit). RM is a powerful technique that takes advantage of the variability in AGN over a range of timescales (from several days to weeks and years; e.g., Peterson et al. 1982)—broad-line region (BLR) response on larger scales to the continuum variations from the accretion disk, with a positive time lag—and provides a way to convert the time lag into a spatial distance, the size of the BLR. The BLR size, along with the width of an emission line, is used to obtain black hole masses in AGN. Successfully applying the RM technique to measure AGN black hole masses thus requires accurate measurements of the emission-line widths. A majority of the low-redshift AGN exhibit broad emission lines (e.g., Hβ, Hα, C IV, etc.) with FWHM $\geqslant 2000$ km s^{-1} in their spectra. Recent efforts by the Super-Eddington Accreting Massive Black Holes (SEAMBH) collaboration (Du et al. 2014, 2015, 2016a, 2016b, 2018; Wang et al. 2014; Hu et al. 2015) have successfully identified ~20 highly accreting AGN to date. The SEAMBH objects show spectral features containing narrower Hβ broad lines (FWHM$_{H\beta} \lesssim 2000$ km s^{-1}), weak [O III], and strong optical Fe II emission lines that appear as a bumpy pseudocontinuum, similar to other NLS1s (Osterbrock & Pogge 1987; Boroson & Green 1992; Boller et al. 1996; Véron-Cetty et al. 2001). As we branch out to studying different categories of AGN, and given the importance of accurate line measurements for RM analysis, we must carefully reconsider: (1) how does spectral resolution influence the shapes of emission lines in our data, and (2) are the current methods of measuring emission-line properties sufficient, or are they limited in any way to achieving our desired science goals?

The aim of this paper is to address the above two questions with the optical spectra of the super-Eddington AGN Markarian 142 (Mrk 142), taken with the Gemini North Observatory (Gemini) and the Lijiang Telescope (LJT). As a part of the broader RM campaign, Cackett et al. (2020)

performed overlapping photometric and spectroscopic observations of Mrk 142 with telescope facilities worldwide. The goal of the campaign is to study the structure of the accretion disk and the BLR simultaneously, for the first time, in a super-Eddington AGN. Because the spectral observations of Mrk 142 with Gemini suffered from gaps due to unfavorable weather, the Gemini observations were complemented with simultaneous observations from LJT. With the Gemini+LJT data, an ultraviolet (UV) continuum to Hβ lag for the object was measured for the first time (Khatu et al. 2022). The Gemini and LJT spectra were taken with the same grating but different slit widths, 0$\overset{''}{.}$75 for Gemini and 2$\overset{''}{.}$5 for LJT; therefore, their spectral resolutions (corresponding to the instrumental FWHMs) differed, 185.6 ± 10.2 km s^{-1} for Gemini and 695.2 ± 3.9 km s^{-1} for LJT. Here the challenge was to accurately measure the emission lines for spectra at considerably different spectral resolutions for a narrow-line object. In this paper, we discuss how to address this challenge with our spectral fitting procedure. Further, we provide recommendations of the best strategies for performing accurate emission-line measurements in narrow-line AGN.

This paper is organized as follows. Section 2 details the process of preparing the data for correlation analysis and the correlations between the Gemini and LJT spectral measurements. Section 3 outlines the results. We discuss the results in Section 4 along with our recommendations. Section 5 summarizes our findings.

2. Methodology

We preprocessed the Gemini and LJT calibrated spectra independently through `PrepSpec`[9] (developer: K. Horne) to correct for any relative deviations from their calibrations. We then modeled the continuum and emission lines in the spectra with `Sherpa`[10] (Freeman et al. 2001) v4.10.0 with a `Python` wrapper script to examine the correlations between the Gemini and LJT spectral measurements.

2.1. `PrepSpec` Preprocessing

`PrepSpec` corrects for differences in the relative wavelength and flux calibrations of the spectra by modeling their continuum, emission lines, and absorption lines. However, `PrepSpec` requires that spectra have no gaps in wavelength and extremely large flux values, for example, resulting from cosmic-ray hits. To prepare the Gemini spectra for `PrepSpec`,

---

[9] `PrepSpec` is a spectral analysis software that fits the continuum and emission lines in the input spectra with a composite model through an iterative process while correcting for any relative deviations in the calibrated wavelength and flux scales of the spectra. See Section 2.1 for more details.

[10] `Sherpa` is a software application for modeling and fitting astronomical images and spectra. In this work, the `Sherpa` v4.10.0 application was used within Coronagraphic Imager with Adaptive Optics (`CIAO`) v4.10.0, the X-ray data analysis software designed by the Chandra X-ray Center. For full documentation of `CIAO`-`Sherpa`, see https://cxc.harvard.edu/sherpa4.14/.

we applied the following corrections: (1) replaced detector gaps and residual features from cosmic-ray correction and sky subtraction with interpolated and simulated data; (2) recovered the flat spectral regions with zero flux values (resulting from the position angle of the slit nonparallel to the parallactic angle) and bumpy regions (resulting from the calibration process) by using a high signal-to-noise ratio (S/N) mean spectrum as the reference spectrum; and (3) recovered slit losses (resulting from the $0''75$ narrow slit used for observations) using $5''00$ wide-slit spectra taken on the same nights. We developed multiple scripts in `Python` v3.6.5 to perform the above corrections. All `Python` scripts are publicly available in the `GitHub` repository *prepdataps* (https://github.com/Virachan/prepdataps). Information on the usage and citation of the scripts is provided in the repository. The LJT spectra had no gaps and hence were directly processed through `PrepSpec` after calibration. The `GitHub` repository includes the user manual for `PrepSpec`, including a detailed tutorial with the Mrk 142 Gemini data set.

2.2. Gemini/LJT Correlation Analysis

We investigated correlations between the Mrk 142 Gemini and LJT emission-line measurements to study the effect of low spectral resolution on the measured FWHM values. To fit the $H\beta \lambda 4861$ and He I $\lambda 5877$ regions of interest, we initially followed a standard approach. We set the FWHM, flux, and position of the [O III] $\lambda 5008$ line to vary during the fit and fixed the FWHMs and positions of the narrow components in Hβ and He I relative to the [O III] $\lambda 5008$ line. We kept the Hβ and He I narrow-line fluxes as free parameters. Further, we used two Gaussians to model the broad Hβ and He I emission lines. We fixed the FWHM of the broader broad Hβ component and allowed the width of the narrower broad component to be a free parameter to reduce the number of free parameters and avFoid degeneracy in the spectral model. For the He I line, we fixed the FWHMs of both of its broad components with respect to the FWHM of the flexible, narrower broad Hβ component. We applied the Boroson & Green (1992) template to fit the Fe II pseudocontinuum and the Bruzual & Charlot (2003) host galaxy template with 11 Gyr at $z = 0.05$ to correct for the effect of host galaxy emission. This approach worked well for the Gemini spectra. However, the LJT Hβ FWHM measurements were broader than expected, indicating that the fitting approach failed for the LJT spectra. Figures 1 and 2 show model fits to a single-epoch spectrum from Gemini and LJT, respectively.

Due to the low resolution of the LJT spectrum ($695.2 \, \mathrm{km \, s}^{-1}$), emission-line features appear smeared as compared to the Gemini spectrum ($185.6 \, \mathrm{km \, s}^{-1}$). In H$\beta$, the sharper peak of the narrow component evident in the Gemini spectrum is not clearly distinguishable in the LJT spectrum. The Fe II emission-line component on the red side of Hβ also appears to contaminate the broader Hβ component. Similarly,

the red wing of the [O III] $\lambda 5008$ line appears to be blended with the Fe II emission on its red side. The possible contamination with Fe II emission due to the low spectral resolution of the LJT spectra results in a broad FWHM for the [O III] $\lambda 5008$ line. Further, at the instrumental resolution of the LJT spectrograph, the [O III] lines with FWHM $\sim 320 \, \mathrm{km \, s}^{-1}$ (as measured from the higher-resolution Gemini spectra) are unresolved. The unresolved [O III] lines in the LJT spectra further complicate the measurements of their widths.

2.2.1. The Problem, Posed: Why Do the Broad Hβ FWHMs from the Gemini and LJT Spectra Not Match?

We found that the FWHM values of the broad Hβ and the [O III] $\lambda 5008$ lines in the Gemini and LJT spectra did not agree with each other. Figure 3 displays the differences in the measured FWHMs of the two lines. To understand the cause of this problem, it is important to consider the differing instrumental resolutions of Gemini and LJT. We used the spectra of a G-type comparison star, common for both the Gemini and the LJT data, observed in the same slit as the target for every exposure to calculate the instrumental resolutions. The comparison star, similar to the target, appears pointlike in the slit and does not fill the entire slit, unlike arc lamp spectra or sky lines; therefore, unresolved absorption lines in the stellar spectra can be used to estimate the line-spread function of the instrument more accurately than arc lamp spectra or sky lines. We fit the weak and hence unresolved Hβ stellar absorption line close to the Hβ/[O III] complex in the Gemini data using a Gaussian function, where the FWHM of the Gaussian gave a mean resolution of $185.6 \pm 10.2 \, \mathrm{km \, s}^{-1}$ with reference to the [O III] $\lambda 5008$ line. Following the procedure in Du et al. (2016a), we convolved a higher-resolution stellar template spectrum with a Gaussian function to obtain the observed stellar spectra in the LJT data; here as well, the FWHM of the convolved Gaussian provided a mean resolution of $695.2 \pm 3.9 \, \mathrm{km \, s}^{-1}$ for the LJT spectrograph. Considering the difference in the resolutions of the Gemini and LJT spectra, we expect the FWHM values from LJT to have a $670.0 \, \mathrm{km \, s}^{-1}$ broader effective width (here defined as the width of the Gaussian kernel required to smooth the higher-resolution Gemini spectrum to the lower-resolution LJT spectrum and given by $\sqrt{695.2^2 - 185.6^2}$ for Gaussian profiles) than the Gemini FWHM values. The [O III] $\lambda 5008$ line in the LJT spectra (Figure 3(a)) has $\sim 680 \, \mathrm{km \, s}^{-1}$ broader effective widths than the [O III] $\lambda 5008$ FWHMs measured from the Gemini spectra, as expected from the differing instrumental resolutions of the two telescopes. However, the LJT Hβ broad line shows a much greater effect, $\sim 1450 \, \mathrm{km \, s}^{-1}$ broader effective widths than those measured from the Gemini spectra. The broad He I FWHM measurements were affected in the same way as Hβ. This implies that there are multiple factors influencing the
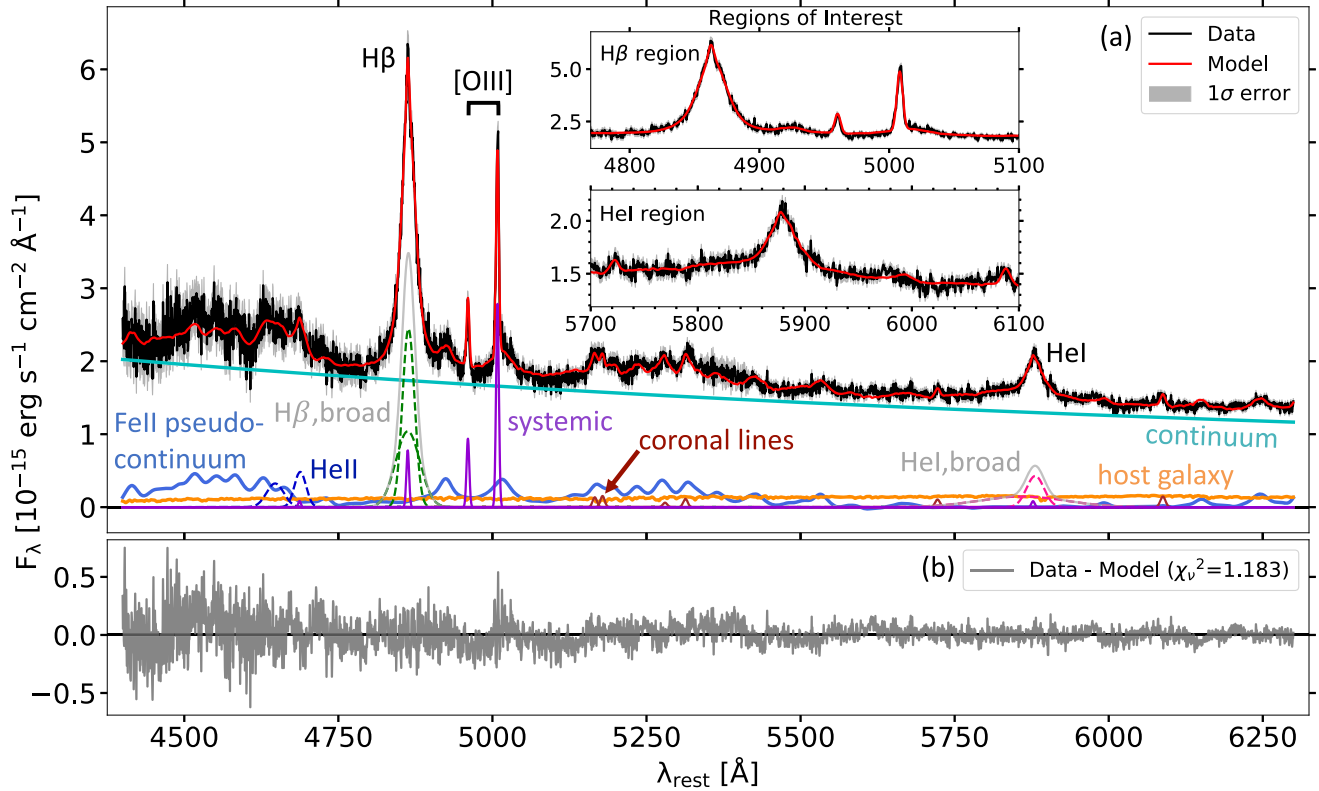
Figure 1. Composite model fit to epoch 24 of the Mrk 142 Gemini data displaying individual components of the model. Panel (a): composite model (red solid curve) fit to the data (black solid curve) from 4430 to 6300 Å in the main panel and Hβ and He I regions of interest in the inset panels. The individual components of the model are displayed at the bottom of the panel: continuum (cyan solid line); Fe II I Zw 1 template as a pseudocontinuum (faint blue solid curve); host galaxy template (orange solid curve); He II broad components (blue dashed Gaussians); Hβ broad components (green dashed Gaussians); He I broad components (pink dashed Gaussians); narrow-line components of Hβ, He I, and [O III] (purple solid Gaussians); and high-ionization coronal lines (brown solid Gaussians). The total broad Hβ and He I profiles are also overplotted (gray solid curves). Panel (b): residuals of the model with reduced χ^2, $\chi_\nu^2 = 1.183$. The model shows larger residuals around the [O III] $\lambda 5008$ line, indicating a suboptimal fit in that region. The noisier blue end of the spectrum affects the overall fit in that region, thus resulting in larger residuals compared to the red end of the spectrum.

FWHM measurements in the LJT spectra, likely resulting from instrumental broadening.

To identify the possible reason(s) for the observed discrepancies in the FWHM measurements, we considered the narrow-line fluxes in the Hβ and [O III] $\lambda 5008$ lines that we allowed to vary during spectral fitting. Figure 4 displays the correlation between the measured fluxes for the two lines. For the LJT spectra, the fluxes in the narrow Hβ line (red open squares) are correlated to the [O III] $\lambda 5008$ line fluxes ($r_{Spearman} \sim 0.5$) with a large scatter in the measured values from both lines. However, the fluxes for narrow lines, originating in the narrow-line region (NLR) of AGN, are not expected to vary relative to the continuum variations over the timescale of an RM campaign. The constancy of the narrow-line fluxes is attributed to the NLR being farther away from the central source (supermassive black hole + accretion disk) than the BLR, which receives the continuum variations. The correlation observed between the LJT narrow Hβ and

[O III] $\lambda 5008$ line fluxes is absent in the Gemini flux values (blue open circles; $r_{Spearman} \sim 0.1$), which are also more constrained than the LJT measurements.

2.2.2. The Culprit, Pronounced: A "Broader" [O III] $\lambda 5008$ FWHM Leads to a Broader Broad Hβ FWHM in the LJT Spectra

Integrating the observations from Figures 3 and 4, we conclude that the "broader" (than expected) [O III] $\lambda 5008$ line in the LJT spectra causes the correlation and scatter observed in the Hβ narrow-line fluxes, consequently leading to the "broader" broad Hβ FWHMs in the LJT spectra as compared to the narrower broad Hβ in the Gemini spectra. The lower spectral resolution of the LJT spectra smears the narrow-line profile of the [O III] $\lambda 5008$ line, causing it to appear broader than usual (see Figure 2). This effect is amplified in the case of Mrk 142, as it is an NLS1 with narrower and weaker [O III] lines compared to the more typical broad-line objects (with
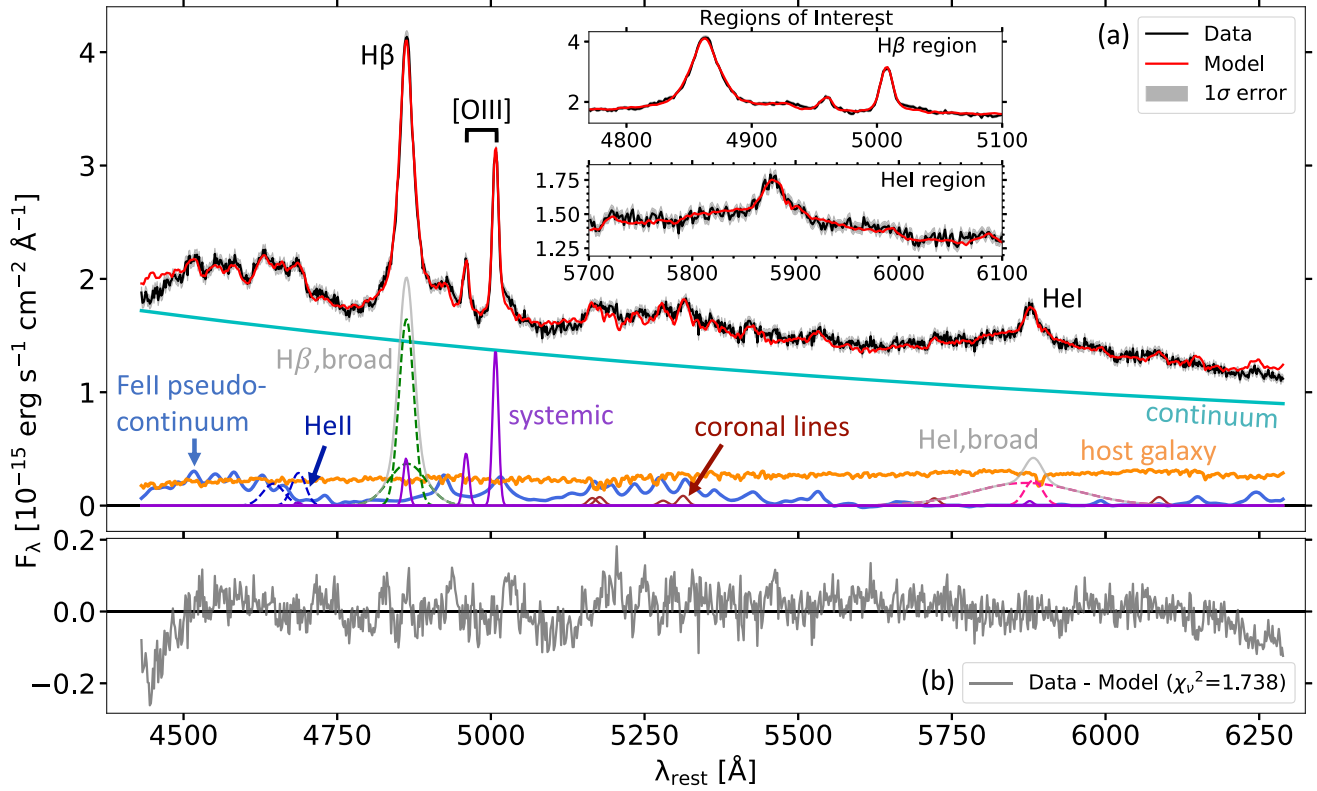
Figure 2. Composite model fit to epoch 24 of the Mrk 142 LJT data displaying individual components of the model. See caption of Figure 1 for a description of the individual model components in panel (a). The red side of the broad Hβ emission line shows contamination with the Fe II emission at ~4923 Å. Similarly, the [O III] λ5008 line shows considerable blending with the Fe II feature in its red wing, thus affecting a reliable measurement of the [O III] λ5008 line. Panel (b) shows the residuals of the model with $\chi_\nu^2 = 1.711$. The smaller residuals indicate an overall good fit to the spectrum. The model performance drops significantly at both ends of the spectrum, although it does not impact measurements in the regions of interest.

narrow-line widths of several hundred kilometers per second). Also, the likely contamination from the Fe II emission at the red wing of [O III] λ5008 (see Figure 2) further complicates the picture. The net result is a "broader" FWHM measured for the [O III] line. We interpret this result to mean the following.

Because the width of the narrow Hβ component is set equal to the width of the [O III] line, a "broader" [O III] leads to a "broader" narrow Hβ in the LJT spectra. The "broader" narrow Hβ collects more flux, leaving less flux for the broad Hβ components, which are kept flexible in the model. The more flux in the narrow Hβ line, lowers the peak flux of the broad Hβ (after subtracting the narrow component), resulting in a "broader" broad Hβ FWHM.

2.2.3. The Solution, Proposed: Tie the Flux in Narrow Hβ Relative to the Flux in [O III] λ5008

To contain the effect of the "broader" [O III] λ5008 line on the broad Hβ FWHM measurements in the LJT spectra, we fixed the narrow-line fluxes, as well as the widths of Hβ and He I relative to the [O III] flux from the Gemini spectral measurements. At the resolution of the Gemini spectra (185.6 km s⁻¹), the [O III] λ5008 line is just resolved. Thus, the FWHM measurements for the [O III] line in the Gemini spectra are more reliable than the LJT values. We therefore applied the narrow-line flux ratios, $F_{H\beta}/F_{[O\ III]\ \lambda5008} = 0.293$ and $F_{He\ I}/F_{[O\ III]\ \lambda5008} = 0.034$, from the Gemini spectra to the Hβ and He I lines, respectively, in the LJT spectra.

Tying the LJT narrow-line flux ratios confined the flux measured for the Hβ narrow component as compared to the Hβ narrow-line flux measured when the narrow-line flux ratios were kept flexible. Figure 4 displays the fixed Hβ narrow-line fluxes from the LJT spectra (red filled squares) as exactly correlated ($r_{Spearman} = 1.0$) to the LJT [O III] λ5008 fluxes. The large scatter in the narrow Hβ line fluxes from flexible line ratios for the LJT spectra (red open squares; $\sigma^2 = 4.631$) is considerably reduced after adopting fixed narrow-line ratios ($\sigma^2 = 0.042$). This reduction in scatter signifies that the Hβ narrow-line fluxes in the LJT spectra are now well constrained. The applied flux ratios along with fixed widths for the narrow lines helped constrain the narrow Hβ flux. With a fixed width
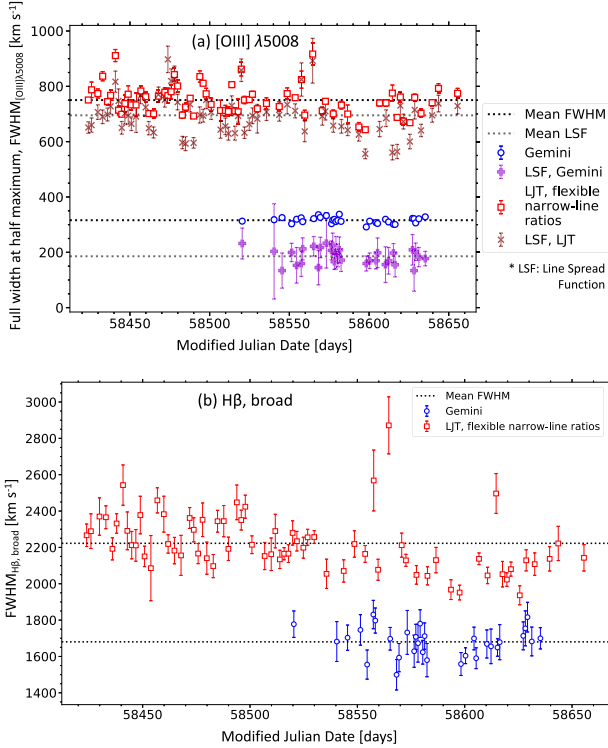
Figure 3. Differences in the FWHM values measured from the Gemini (blue open circles) and LJT (red open squares) spectra for [O III] λ5008 (panel (a)) and broad Hβ (panel (b)), indicating that the LJT measurements have a broader effective width of 670.0 km s^{-1} (see text for the definition), as expected owing to the Gemini and LJT instrumental resolutions. In panel (a), the purple plus signs and maroon crosses represent the line-spread functions (determined from the comparison star observed in the same slit as the target at each epoch) for the Gemini and LJT data, respectively. The fitting procedure for both the Gemini and LJT spectra incorporated a flexible narrow-line ratio of Hβ to [O III] λ5008.

and constrained flux of the narrow Hβ component, the "excess" flux is directed back to the broad components. The flux gained by broad Hβ causes, the higher the peak flux measured for the broad Hβ to rise higher, resulting in a narrower broad Hβ FWHM.

3. Results

We studied the effect of the LJT spectral resolution (695.2 km s^{-1}) on the measured Hβ FWHMs by correlating the emission-line measurements in the Mrk 142 Gemini and LJT spectra. We identified that the "broader" FWHM measurements of the unresolved [O III] λ5008 line in the LJT spectra lead to an overestimation of the Hβ narrow-line fluxes by a factor of 2, ultimately resulting in Hβ FWHM values with an $\sim$1450 km s^{-1} broader effective width than the Hβ FWHM values from the Gemini spectra. To correct for this effect, we adapted our spectral fitting procedure for the LJT spectra by fixing the narrow-line ratios of Hβ and He I with respect to the [O III] λ5008 line based on our spectral measurements for the
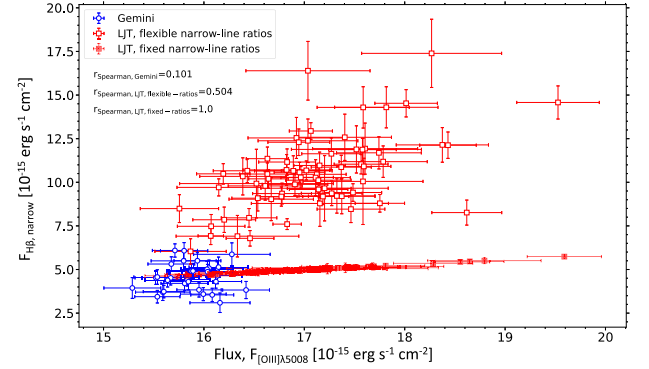

Figure 4. Correlations between the narrow Hβ line flux and the [O III] λ5008 line flux from the Gemini (blue circles) and LJT (red squares) spectra. Open symbols represent measurements with flexible narrow-line flux ratios of $F_{H\beta}/F_{[O\ III]\ \lambda5008}$ and $F_{He\ I}/F_{[O\ III]\ \lambda5008}$, whereas filled symbols (for LJT only) represent measurements with fixed narrow-line flux ratios. For fitting the LJT spectra, we fixed the above narrow-line flux ratios determined from the Gemini spectra fitting process (0.293 for Hβ to [O III] λ5008 and 0.034 for He I to [O III] λ5008), as the resolved [O III] λ5008 line in the Gemini spectra provided reliable measurements of the narrow-line flux ratios. The weak positive correlation for the LJT measurements with flexible narrow-line ratios indicates that the "broader" [O III] λ5008 line results in an excess narrow-line flux for the narrow Hβ component.

Gemini spectra containing resolved [O III] lines. We present our results below.

Applying narrow-line flux ratios for fitting the lower-resolution LJT spectra significantly reduces the scatter in the narrow-line fluxes of the Hβ and He I broad lines. Figure 5 displays the fluxes of the narrow component in Hβ (panel (a)) and He I (panel (b)) before and after applying the flux ratios for the LJT spectra. Before fixing the narrow-line fluxes, the higher Hβ to [O III] λ5008 and He I to [O III] λ5008 flux ratios for the lower-resolution LJT spectra result from the "excess" flux gathered under the narrow Hβ and He I lines owing to the narrow Hβ and He I line widths set equal to the width of the "broader" [O III] λ5008 line. After fixing the narrow-line flux ratios, the Hβ and He I line measurements are more consistent, with values similar to the narrow-line fluxes from the Gemini data. The higher resolution of the Gemini spectra, providing resolved [O III] lines, allowed precise measurements of [O III] line widths and fluxes, thus resulting in the smaller scatter in the Hβ and He I narrow-line fluxes. In addition, we expect the narrow-line fluxes to be constant over the length of our campaign. However, the Hβ and He I narrow-line fluxes from the LJT spectra are unreliable when the narrow-line ratios are free parameters due to the large uncertainties and scatter in the measured values. The constant Hβ and He I narrow-line flux is clearly evident after fixing the narrow-line ratios for the LJT spectra.

We found that the constrained Hβ narrow-line fluxes in the LJT spectra yield narrower FWHMs for the Hβ broad
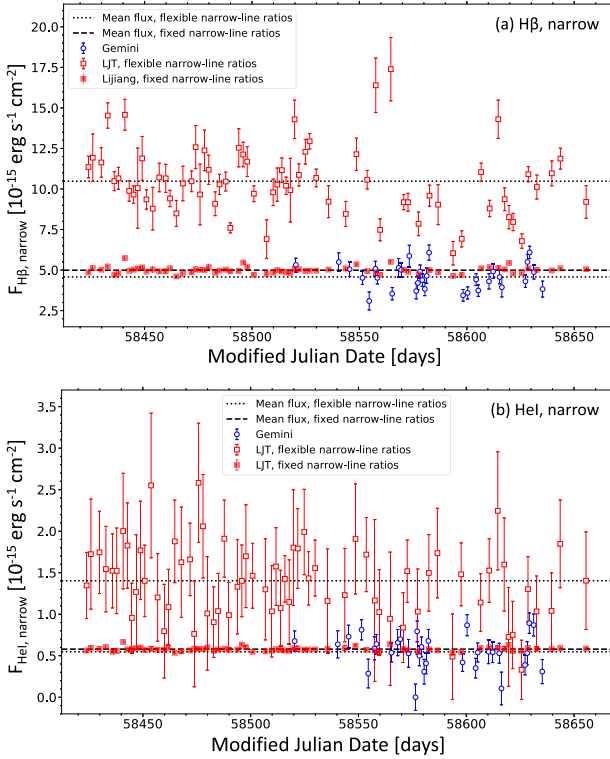
Figure 5. Narrow Hβ (panel (a)) and He I (panel (b)) light curves measured from the Gemini (blue circles) and LJT (red squares) spectra fit with flexible (open symbols) and fixed (filled symbols) narrow-line flux ratios. Fixing the Hβ and He I narrow-line flux ratios of 0.293 and 0.034, respectively, relative to the [O III] λ5008 line flux considerably reduced the scatter in the LJT measurements and resulted in lower uncertainties. With fixed narrow-line flux ratios, the new fluxes for the narrow Hβ and He I lines from the LJT spectra are closer to the Gemini measurements.

Figure 6. Correlations between the broad Hβ FWHM and the narrow Hβ flux from the Gemini (blue circles) and LJT (red squares) spectra fit with flexible (open symbols) and fixed (filled symbols) narrow-line flux ratios. The scatter in the LJT measurements with flexible narrow-line ratios (orange shaded region) is considerably reduced (red shaded region) after fixing the narrow-line ratios. Fixed ratios nullified the strong correlation that is evident in the LJT measurements with flexible ratios.

Figure 7. Dependence of the FWHM on the peak flux of the broad Hβ line from the Gemini (blue circles) and LJT (red squares) spectra fit with flexible (open symbols) and fixed (filled symbols) narrow-line flux ratios. Fixed ratios nullified the strong correlation that is evident in the LJT measurements with flexible ratios.

component, and Figure 6 displays this result. Flexible narrow-line flux ratios in the LJT spectra result in a large scatter in the broad Hβ FWHMs (red open squares) with a mean value of $\sim$2220 km s^{-1}. After fixing the narrow-line flux ratios, the constrained narrow-line flux in Hβ reallocates the "excess" flux to the broad components. As a result of the higher broad-line peak flux, the half-maximum point increases, thus measuring a narrower Hβ broad-line profile. Figure 7 explicitly shows the dependence of the measured Hβ FWHM on the peak flux of the line. With flexible narrow-line ratios for the lower-resolution LJT spectra, the measured broad Hβ FWHMs are strongly negatively correlated ($r_{\rm Spearman} = -0.789$) with the peak fluxes of the line. This correlation is weaker ($r_{\rm Spearman} = -0.449$) with the fixed narrow-line flux ratios for the LJT spectra and also similar to the correlation observed for the Gemini spectra ($r_{\rm Spearman} = -0.487$). The remaining dependence of the broad Hβ FWHM on its peak flux can be attributed to the contamination in the Hβ line from the nearby Fe II emission (also discussed below). The new measurements of the broad
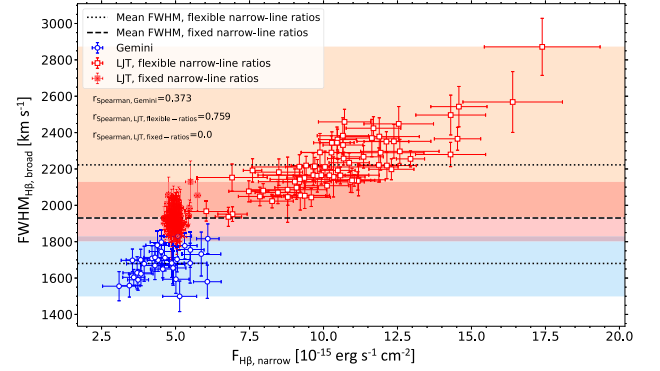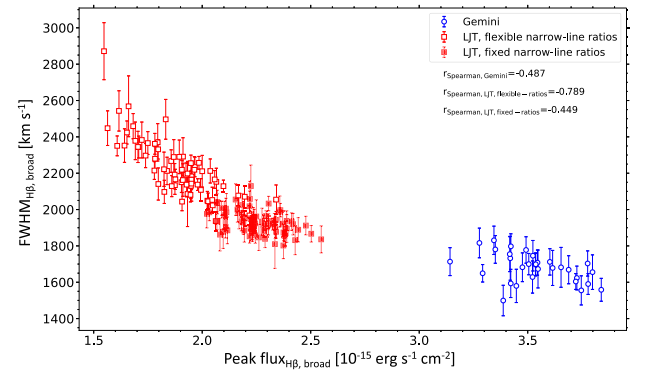
Hβ FWHM, obtained after fixing the narrow-line flux ratios for the LJT spectra, have a mean of $\sim$1930 km s^{-1}, $\sim$54% closer to the Gemini Hβ mean FWHM. The new broad Hβ FWHM values also show a scatter of $\sim$340 km s^{-1}, similar to the scatter in the Gemini Hβ FWHM values (see Figure 6).

We also examined the correlation between the strength of Fe II ($R_{\rm Fe\ II}$, defined as the ratio of the equivalent width of Fe II in the 4434–4684 Å region to that of broad Hβ) and the FWHM of broad Hβ, shown in Figure 8. The $R_{\rm Fe\ II}$–FWHM$_{\rm H\beta, broad}$ correlation reiterates the issue of the broader Hβ FWHM measurements in a different context. The LJT Hβ FWHM values with flexible narrow-line ratios (red open squares) are weakly correlated to $R_{\rm Fe\ II}$. This correlation vanishes after fixing the narrow-line flux ratio of Hβ to [O III] λ5008. The new
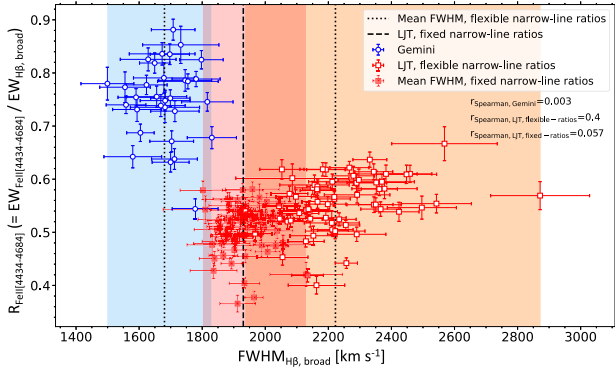
Figure 8. Correlations between the strength of Fe II (ratio of the equivalent width of Fe II in the [4434–4684 Å] region to that of broad Hβ) and the FWHM of the broad Hβ from the Gemini (blue circles) and LJT (red squares) spectra fit with flexible (open symbols) and fixed (filled symbols) narrow-line flux ratios. Fixing the narrow-line flux ratios moved the mean Hβ FWHM from the LJT data closer to the mean of the Gemini Hβ FWHM measurements. There is an unexplained offset between the Gemini and new LJT measurements, likely due to the Fe II emission contaminating the broad Hβ line in the LJT spectra.

broad Hβ measurements (red filled squares) are closer to the values measured from the Gemini spectra; however, an offset is still present. At the low spectral resolution of the LJT spectra, the Fe II emission around the Hβ line likely contaminates the Hβ broad-line emission (see Figure 2). The remainder offset noted above can likely be a result of the potential Fe II contamination with the broad Hβ line in the LJT spectra. Therefore, understanding any interplay between the two lines is crucial. In addition, we note that the $R_{Fe II}$ measurements from the LJT spectra are smaller compared to those from the Gemini spectra, likely due to the lower resolution of the LJT data.

4. Discussion

We correlated emission-line measurements from Mrk 142 spectra taken with Gemini and LJT at different resolutions (185.6 km s^{-1} for the former and 695.2 km s^{-1} for the latter) to study the discrepancies observed in the measured FWHM values of broad Hβ. Given the NLS1 nature of Mrk 142, its broad Hβ profile is narrower compared to the more typical broad-line Seyfert 1s and therefore challenging to accurately measure in lower-resolution spectra. Accurate measurements of the narrow-line fluxes are critical to measure broad emission-line widths, which in turn are used to derive the black hole masses in AGN.

Our adopted method of measuring the broad Hβ FWHM decreased the FWHM values measured from the LJT spectra significantly, thus bringing them closer to the Gemini measurements, as well as reducing the scatter in the measured values. The smaller scatter in the Hβ FWHMs from the LJT spectra was an improvement by a factor of ∼2.6 compared to the measurements with flexible narrow-line ratios. Although we

significantly improved our measurements from the LJT spectra, the new Hβ FWHM values do not exactly match those from the Gemini spectra. There is an offset of ∼250 km s^{-1} between the mean FWHM values from the two data sets that is perhaps a consequence of the Fe II emission contaminating the broad red wing of Hβ. At lower resolution, the strong Fe II lines in the LJT spectra are smeared compared to the sharper features in the Gemini spectra (see Figures 1 and 2), resulting in weaker Fe II measured from the LJT spectra (see Figure 8). Therefore, there likely exists cross talk between the two broad lines affecting the measurements of both the Fe II emission and the broad Hβ wings.

We also caution that our method does not affect the [O III] line measurements from the LJT spectra, although it restores the broad-line flux measured for the Hβ line. Figure 9 makes this explicit. The [O III] fluxes measured from the LJT spectra are approximately the same (red filled squares) before fixing the narrow-line flux ratios (see Figure 9(a)). The [O III] fluxes remain unchanged because the [O III] λ5008 flux was freed during spectral fitting. In contrast, an increase in flux is clearly seen in the broad Hβ light curve (red filled squares in Figure 9(b)). Fixing the narrow-line flux ratios resulted in an increase of ≲10% in the Hβ broad-line flux in the LJT spectra, a difference that is greater than or similar to the Hβ flux uncertainties in a majority of the LJT epochs. Our proposed method here can be used with spectral data sets having different resolutions from either different gratings or different slit widths. However, it does not test the effect on line fluxes, e.g., the offset observed in the broad Hβ line fluxes from Gemini and LJT (see Figure 9(b)). Such an offset may result from varying slit widths or orientation of the slit or be a combined effect of both. The orientation effect can be especially concerning for extended sources in which the [O III] emission emerging from the NLR on larger spatial scales and the broad Hβ emission from the BLR closer to the central black hole can fill the slit differently. However, the size of the central source in Mrk 142 is 3″ × 3″ (and the apparent size of the host galaxy is 15″ × 15″), where the issue of Hβ/[O III] emission filling the slit differently on a spatial scale is likely negligible. Nevertheless, we note that testing our proposed method with different slit widths and orientations will help with understanding the effects on measured line widths and fluxes in greater detail.

In general, the rms spectra do not suffer from the blending of broad- and narrow-line features because the variable part of the spectrum is exclusively from the BLR. However, rms spectra are noisier compared to the spectra from individual epochs; the emission-line widths obtained from rms spectra have higher uncertainties. Therefore, we considered measuring Hβ broad-line widths from individual-epoch Gemini and LJT spectra.
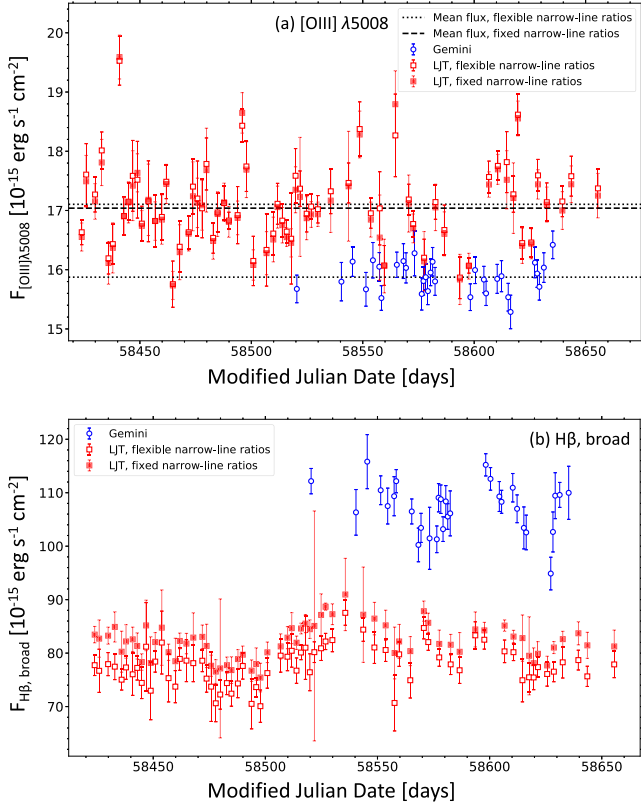
Figure 9. The [O III] $\lambda 5008$ (panel (a)) and broad Hβ (panel (b)) light curves from the Gemini (blue circles) and LJT (red squares) spectra fit with flexible (open symbols) and fixed (filled symbols) narrow-line flux ratios. Because the [O III] $\lambda 5008$ line flux is kept flexible even while fitting with fixed narrow-line flux ratios, the measured fluxes before and after fixing narrow-line ratios are similar for the [O III] line. However, there is an $\sim 10\%$ increase in the the broad Hβ flux from the LJT spectra fit with fixed narrow-line ratios.

4.1. Comparison to Previous Studies

We compared our methodology to the techniques used in previous studies. In a previous SEAMBH monitoring campaign with LJT (Du et al. 2014; Hu et al. 2015), Mrk 142 spectra were taken with the same instrument settings as used for the data set in this work. Hu et al. (2015) described the spectral fitting technique adopted for measuring Hβ FWHM from the previous campaign. They followed a two-step process. (1) Assuming no narrow-line contribution in the Hβ emission and given that the narrow lines do not vary at the short variability timescales of the broad-line gas, they modeled the Hβ profile with a Gauss–Hermite function. (2) They modeled the Hβ narrow line with a Gaussian whose width was set equal to that of the [O III] $\lambda 5008$ line and position fixed relative to the [O III] line. They ran their fits in two cycles: first, assuming 10% of the [O III] $\lambda 5008$ flux for the narrow Hβ component, and the value of the broad Hβ FWHM was used from this run; and second, assuming 20% narrow-line flux, and the uncertainty on

the FWHM measurement was used from this run in addition to the uncertainty from the Gauss–Hermite fit for the line. While the calibration of the uncertainties on the measured Hβ FWHMs from the two-cycle and Gauss–Hermite fits appears sufficient, the flux ratio of the Hβ to [O III] narrow lines is somewhat arbitrarily defined. As the narrow-line flux ratios can be different for different objects, using arbitrary ratios or even the same ratios for different objects can result in a systematic overestimation or underestimation of the broad Hβ FWHM values. With the opportunity of using Mrk 142 spectra at two different resolutions, we applied the more reliable narrow-line flux ratios determined from the higher-resolution and high-S/N Gemini spectra to the lower-resolution LJT spectra for the Hβ FWHM measurements from the latter.

Two of the proposed methods of correcting for the effect of different spectral resolution on line width measurements are (1) fitting a difference spectrum between an input spectrum, whose flux scale factor (or flux ratio) is to be determined, and a reference spectrum, typically a high-S/N spectrum (van Groningen & Wanders 1992); and (2) subtracting the rms width of the line-spread function of the spectrograph from the observed line profile (Fausnaugh et al. 2017). In the method by van Groningen & Wanders (1992), if the input and reference (at higher resolution) spectra have different resolutions, the algorithm first finds a convolution factor to degrade the reference spectrum and then determines the scale factor by fitting a simple analytical function to the difference spectrum that is nonvariable over the spectral regions of narrow lines. However, the success rate of determining the scale factor for the correct input spectrum decreases as the difference in the spectral resolution decreases. For the latter case, the method suggested in this work provides a robust way of measuring the line width by first calculating the flux scale factor from a higher-resolution spectrum and then applying it to lower-resolution spectra, thus providing a robust way to work with spectra having less dissimilar resolutions. An alternative method by Fausnaugh et al. (2017) attempts to first determine the line-spread function of the spectrograph to subtract from an observed profile so that the intrinsic line width is measured more accurately, especially for low-resolution spectra. However, determination of a spectrograph's line-spread function relies on a prior measurement of a narrow-line profile for at least one of the objects in the data set (e.g., the Whittle 1992 database used by Fausnaugh et al. 2017). Furthermore, using a previous database value to correct for the spectrograph's line-spread function does not necessarily catch the temporal variations in the instrument behavior, where narrow-line ratios from high-resolution spectra taken on the same night as the low-resolution spectra, as in this work, are beneficial for accurate measurement of the line width.

Additionally, past studies discuss the use of different line width measures for reliable black hole mass estimates (Liu & Bian 2022). Peterson et al. (2004) conducted a time-series

analysis of 35 AGN to test the effectiveness of different line width measures for calculating black hole masses. They concluded that the line dispersion (σ_{line}; or the rms width calculated from the second moment of a line profile) is a more robust measure of the variable line profile than FWHM, especially in objects with strong narrow lines. However, Bian et al. (2008) argued that σ_{line} strongly depends on the contribution from the wings of broad lines. They analyzed 329 NLS1s from the Sloan Digital Sky Survey catalog to determine their black hole masses using σ_{line}. They inferred that in the cases where the Hβ broad profile is defined by two broad components (as for Mrk 142 spectra in this work), the black hole mass measurements using σ_{line} are about 0.5 dex larger than those obtained from FWHM measurements.

In another study, Collin et al. (2006) characterized the broad Hβ emission-line profiles of all reverberation-mapped AGN - based on the ratio of FWHM/σ_{line},[11] separating the AGN with narrower broad Hβ profiles (FWHM/$\sigma_{line} < 2.35$) from those with broader Hβ (FWHM/$\sigma_{line} > 2.35$). In their analysis of the virial product (VP $= M_\bullet/f$, where f is the scale factor) with the FWHM and σ_{line} from both mean and rms spectra, they showed that (1) although σ_{line} yields consistent results for scale factors from both the mean and the rms spectra for objects with narrower as well as broader broad Hβ profiles, σ_{line} from the mean spectrum is, on average, ~20% broader in the mean than in the rms spectra; and (2) for the narrower broad Hβ population (including NLS1s), although the scale factors from the FWHM are larger by a factor of ~3 from both mean and rms spectra, the FWHM is only ~10% broader in the mean than the rms spectra. It is worth noting from the above discussions that both the FWHM and the σ_{line} are typically measured to be broader in the mean than the rms spectra.

4.2. Recommendations for Line Width Measurements in Narrow-line AGN

The discrepancies highlighted by previous studies emphasize that accurately measuring broad-line widths in narrow-line objects, e.g., NLS1s, is not straightforward. As demonstrated in this work, the flux leak from the broad-line to the narrow-line components can significantly affect the measured FWHM of the broad lines, e.g., Hβ, in NLS1s. The flux leak from Fe II around Hβ can also affect the Hβ FWHM measurements. A consistent watch on how the quality of the data and the measurement methods influence each other is essential. Surrounded by Fe II emission in the optical and the [O III] $\lambda\lambda4960$, 5008 lines, Hβ is challenging to measure; however, it is accessible to most of the ground-based observatories over a considerably wide redshift range and therefore prominently used for RM studies. Based on our

---

[11] The nature of a broad-line profile determines the relationship between the FWHM and σ_{line}, where FWHM/$\sigma_{line} = 2.35$ for a Gaussian profile.

analysis in this work, we provide recommendations on measuring emission-line widths in narrow-line AGN.

We strongly recommend both higher- and lower-resolution observations for RM analysis of narrow-line AGN. In RM, the nearest neighboring narrow line is typically used for relative flux calibration of the broad lines of interest; e.g., [O III] $\lambda5008$ is used as a calibrator line for measuring Hβ. Therefore, a completely resolved calibrator line is essential. We regard this as the primary requirement for accurately measuring the broad-line widths in narrow-line AGN. Then, while measuring line profiles, applying narrow-line flux ratios (relative to the calibrator line) determined from the higher-resolution spectra will allow more accurate measurements of line widths with the mean spectra. If only lower-resolution spectra are available, we recommend using higher-resolution spectra from archival observations to determine the appropriate narrow-line flux ratios. If no archival higher-resolution spectra exist, we highly recommend scheduling at least one higher-resolution spectrum along with lower-resolution spectra at each epoch. An RM analysis of narrow-line AGN will benefit extensively from simultaneous higher- and lower-resolution observations.

5. Conclusion

We performed a detailed correlation analysis of the spectral measurements from the Mrk 142 data taken with Gemini at higher resolution (185.6 km s^{-1}) and LJT at lower resolution (695.2 km s^{-1}) to understand the effect of different spectral resolutions on the measured physical properties of emission lines. The FWHMs measured for the broad Hβ from the Gemini and LJT spectra did not overlap. Through our analysis, we identified that the "broader," unresolved [O III] $\lambda5008$ in the LJT spectra affected the Hβ FWHM measurements during spectral fitting. We corrected for the LJT Hβ FWHM values by fixing the narrow-line flux ratio of Hβ to the [O III] $\lambda5008$ line flux as determined from the Gemini spectral fits. Adopting this procedure, the mean Hβ FWHM reduced from ~2220 to ~1930 km s^{-1}, an improvement of ~54% in the mean value. We summarize our main results below.

1. In Mrk 142, lower-resolution spectra with an unresolved [O III] $\lambda5008$ line and a fixed [O III] $\lambda5008$ width but flexible line flux for the narrow Hβ caused a flux leak from the broad to the narrow component, resulting in a lower peak flux for the broad-line profile and therefore a broader broad Hβ FWHM as compared to the higher-resolution spectra with a resolved [O III] $\lambda5008$ line.

2. Fixing the narrow-line flux ratio of Hβ to [O III] $\lambda5008$ while measuring the Hβ broad-line profile in the LJT spectra nullified the correlation of the broad Hβ FWHM with the [O III] $\lambda5008$ flux and reduced the scatter in the FWHM values by a factor of 2.6, equal to the scatter in the Hβ FWHMs measured from the Gemini spectra. Consequently, the mean of the Hβ FWHM values

decreased by $\sim54\%$, or an effective width of $\sim1000\ \mathrm{km\ s^{-1}}$. The remaining offset is likely from Fe II.

3. Considering the impact of a resolved [O III] $\lambda5008$ on the Hβ FWHM measurements, we strongly recommend using both higher- and lower-resolution spectra for measuring line profiles in narrow-line AGN.

We leveraged the access to both the Gemini and LJT spectra of Mrk 142 for RM analysis; while the LJT observations expanded the time baseline and filled the gaps in the Gemini observations, the Gemini spectra at higher resolution allowed more precise Hβ line measurements from the LJT spectra. We emphasize that measuring broad-line profiles in objects with narrower broad lines than the typical AGN population is not straightforward. Branching out to diverse populations for RM studies perhaps needs a revisit to emission-line measurement methods.

ORCID iDs

Viraja C. Khatu ● https://orcid.org/0000-0002-0581-6506
Sarah C. Gallagher ● https://orcid.org/0000-0001-6217-8101
Keith Horne ● https://orcid.org/0000-0003-1728-0304
Edward M. Cackett ● https://orcid.org/0000-0002-8294-9281
Pu Du ● https://orcid.org/0000-0002-5830-3544
Jian-Min Wang ● https://orcid.org/0000-0001-9449-9268
Wei-Hao Bian ● https://orcid.org/0000-0002-2121-8960
Sha-Sha Li ● https://orcid.org/0000-0003-3823-3419
Yan-Rong Li ● https://orcid.org/0000-0001-5841-9179
Sofia Pasquini ● https://orcid.org/0000-0002-9416-8001

References

Astropy Collaboration, Robitaille, T. P., Tollerud, E. J., et al. 2013, A&A, 558, A33
Bentz, M. C., Denney, K. D., Cackett, E. M., et al. 2006, ApJ, 651, 775
Bian, W.-H., Hu, C., Gu, Q.-S., & Wang, J.-M. 2008, MNRAS, 390, 752
Blandford, R. D., & McKee, C. F. 1982, ApJ, 255, 419
Boller, T., Brandt, W. N., & Fink, H. 1996, A&A, 305, 53
Boroson, T. A., & Green, R. F. 1992, ApJS, 80, 109
Bruzual, G., & Charlot, S. 2003, MNRAS, 344, 1000
Cackett, E. M., Gelbord, J., Li, Y.-R., et al. 2020, ApJ, 896, 1
Collier, S. J., Horne, K., Kaspi, S., et al. 1998, ApJ, 500, 162
Collin, S., Kawaguchi, T., Peterson, B. M., & Vestergaard, M. 2006, A&A, 456, 75
Dietrich, M., Peterson, B. M., Albrecht, P., et al. 1998, ApJS, 115, 185
Du, P., Hu, C., Lu, K.-X., et al. 2014, ApJ, 782, 45
Du, P., Hu, C., Lu, K.-X., et al. 2015, ApJ, 806, 22
Du, P., Lu, K.-X., Hu, C., et al. 2016a, ApJ, 820, 27
Du, P., Lu, K.-X., Zhang, Z.-X., et al. 2016b, ApJ, 825, 126
Du, P., Zhang, Z.-X., Wang, K., et al. 2018, ApJ, 856, 6
Fausnaugh, M. M., Grier, C. J., Bentz, M. C., et al. 2017, ApJ, 840, 97
Freeman, P., Doe, S., & Siemiginowska, A. 2001, Proc. SPIE, 4477, 76
Hu, C., Du, P., Lu, K.-X., et al. 2015, ApJ, 804, 138
Kaspi, S., Smith, P. S., Netzer, H., et al. 2000, ApJ, 533, 631
Khatu, V. C., Gallagher, S. C., Horne, K., et al. 2022, ApJ, submitted
Liu, Y.-S., & Bian, W.-H. 2022, ApJ, 937, 82
Osterbrock, D. E., & Pogge, R. W. 1987, ApJ, 323, 108
Peterson, B. M. 1993, PASP, 105, 247
Peterson, B. M., Ferrarese, L., Gilbert, K. M., et al. 2004, ApJ, 613, 682
Peterson, B. M., Foltz, C. B., Byard, P. L., & Wagner, R. M. 1982, ApJS, 49, 469
Santos-Lleó, M., Chatzichristou, E., de Oliveira, C. M., et al. 1997, ApJS, 112, 271
Stirpe, G. M., Winge, C., Altieri, B., et al. 1994, ApJ, 425, 609
van Groningen, E., & Wanders, I. 1992, PASP, 104, 700
Véron-Cetty, M. P., Véron, P., & Gonçalves, A. C. 2001, A&A, 372, 730
Wang, J.-M., Du, P., Hu, C., et al. 2014, ApJ, 793, 108
Whittle, M. 1992, ApJS, 79, 49